J Math Imaging Vis (2013) 45:55–68
DOI 10.1007/s10851-012-0344-0

On the Curve Reconstruction in Riemannian Manifolds

Ordering Motion Frames

Pratik Shah · Samaresh Chatterji

Published online: 17 May 2012

Abstract In this article we extend the computational geometric curve reconstruction approach to the curves embedded in the Riemannian manifold. We prove that the minimal spanning tree, given a sufficiently dense sample, correctly reconstructs the smooth arcs which can be used to reconstruct closed and simple curves in Riemannian manifolds. The proof is based on the behavior of the curve segment inside the tubular neighborhood of the curve. To take care of the local topological changes of the manifold, the tubular neighborhood is constructed in consideration with the injectivity radius of the underlying Riemannian manifold. We also present examples of successfully reconstructed curves and show applications of curve reconstruction to ordering motion frames.

Keywords Curve reconstruction · Riemannian manifold · Video frame ordering · Ordering rotations

1 Introduction

The curve reconstruction problem can be thought of as *connect the dots*. Idea is quite similar to the Nyquist's sampling theorem for band limited signals in signal processing. The only difference is in terms of ordering of the sample. Unlike in the latter case, the ordering is lost when we have a sample of data points of a curve. Thus the problem of curve reconstruction first requires to establish a proper sampling criterion. Next, to give a provable ordering algorithm based on the suggested sampling criterion. Finally the problem ends with an interpolation scheme to join the samples based on some smoothness constraints. Nature of problem to be dealt with in this article corresponds to the former one. Suppose an object in $\mathbb{R}^3$ is in motion and we have captured some frames of this motion. But these frames are jumbled up, i.e. the ordering is lost. Reconstruct the original motion given that the frames captured form a dense sample set.

Think of a graphic game designer designing a game. To design a path of an object and the way the object moves along that path he must first create a sequence of orientations and displacements in the space. A usual process of animation is to begin with the first frame and the last frame. Graphic designer will create inbetween frames iteratively. Based on movements along the path he may create intermediate frames in an order which best suits his imagination. Now he provides these frames to an interpolator. At this stage he is also required to provide an ordering of the frames to the interpolator.

Results presented in this work provide a way to automate the process of ordering the frames created by a graphic designer. In this work we present a sampling criterion, an ordering algorithm and an interpolation scheme that reconstructs the approximation to the original motion. We have made an attempt to extend the computational geometric curve reconstruction approach to curved spaces (Riemannian Manifolds). Instances of applications of curve reconstruction in curved spaces are sparsely present in literature, see for example, edge grouping in [6], and DT-MRI tractography in [5]. In [6], Voronoi diagram construction is used for perceptual grouping of points on a curved surface.

The Riemannian manifold we are interested in, i.e. the Euclidean motion $SE(3)$, $SE(2)$, are endowed with an additional structure of a group and there by give us Lie groups to work on. $SE(3)$ is a well studied object in physics and math-

P. Shah (✉) · S. Chatterji
Dhirubhai Ambani Institute of Information and Communication Technology, Gandhinagar, India
e-mail: pratik_shah@daiict.ac.in

S. Chatterji
e-mail: samaresh_chatterji@daiict.ac.in

ematics. $SE(2)$ is used to model the set of configurations of an object under Euclidean motion and is explored in the domain of image processing for segmentation as well as in object tracking where one is interested in a constrained evolution of a curve under the action of $SE(2)$, [18]. $SE(3)$ is used extensively in robotics for path planning and motion planning of robots. It is also useful in computer vision and graphics. No bi-invariant metric exist on $SE(3)$. Together with the Riemannian metric defined on it, the *exponential map* and further a left invariant distance metric on $SE(3)$ can be expressed in a closed form. We give examples of successfully reconstructed curves in $SE(2)$ and $SE(3)$. We show an application of curve reconstruction in $SE(2)$ for ordering video frames. We show that for densely sampled curves, *minimal spanning tree* (MST) gives a correct polygonal reconstruction of curves in Riemannian manifolds. It can be shown that the problem of curve reconstruction is equivalent to that of traveling salesman problem. In [2], authors show that in the context of curve reconstruction, the traveling sales man tour can be constructed in polynomial time. Once ordered, we interpolate the ordered point set by a partial geodesic interpolation scheme. To ensure smoothness at the sample points we also propose to interpolate samples using de Casteljau algorithm assuming that the boundary conditions are known. It is possible to tackle a noisy sample both in combinatorial and variational curve reconstruction approaches, see for example [11] and [24]. In this article, we do not discuss issues related to noisy sample.

2 Background

We begin with a quick review of curve reconstruction in the plane, keeping the notations and definitions as general as possible. A curve, for our purpose, is a set of image points of a smooth function $\mathcal{C} : [0, 1] \to \mathcal{M}$. More specifically looking at the application at hand, we restrict $\mathcal{M}$ to be a differentiable manifold. A subclass of curves those are smooth and simple is of vital importance in pattern recognition, graphics, image processing and computer vision.

If $\mathcal{M} = \mathbb{R}^2$ then the problem is of reconstructing curves in a plane and $\mathcal{C}$ is planar. $\mathbb{R}^2$ along with the standard Euclidean distance metric is a metric space. Naturally the question arises: Is it always possible to have a finite sample set $\mathcal{S} \subset \mathcal{C}$ which captures all the details about $\mathcal{C}$? Answer to this question lies in the fact that $\mathcal{C}$ is smooth and is a compact one dimensional submanifold. To appreciate further let us look at the definition of an ε-net. For given $\varepsilon > 0$, a subset $\mathcal{S}$ of $\mathcal{C}$ is called an ε-net if $\mathcal{S}$ is finite and $\mathcal{C} \subset \bigcup_{s \in \mathcal{S}} B_\varepsilon(s)$, where $B_\varepsilon(s)$ is an open ball in $\mathcal{M}$ with radius ε. In other words $\mathcal{S}$ is finite and its points are scattered through $\mathcal{C}$ in such a way that each point of $\mathcal{C}$ is at a distance less than ε from at least one point of $\mathcal{S}$. Since $\mathcal{C}$ is compact every cover will have a finite sub-cover, which shows a possibility of a finite representative sample set of $\mathcal{C}$. The concept of ε-net captures the idea of sampling criterion very well.

In [11], based on the uniform sampling criterion an Euclidean MST is suggested for the reconstruction. In the initial phase of the development, uniform sampling criterion was the bottleneck. The first breakthrough came with the non-uniform sampling criterion suggested based on the local feature size by [4]. Unlike the uniform sampling it samples the curve more where the details are more. Non-uniform sampling of a curve is based on the medial axis of that curve. The *medial axis* of a curve $\mathcal{C}$ is closure of the set of points in $\mathcal{M}$ which have two or more closest points in $\mathcal{C}$. A simple closed curve in a plane divides the plane into two disjoint regions. Medial axis can be thought of as the union of disjoint skeletons of the regions divided by the curve. The *Local feature size*, $f(p)$, of a point $p \in \mathcal{C}$ is defined as the Euclidean distance from p to the closest point on the medial axis.

$\mathcal{C}$ is *ε-sampled* by a set of sample points $\mathcal{S}$ if every $p \in \mathcal{C}$ is within distance $\varepsilon \cdot f(p)$ of a sample $s \in \mathcal{S}$. The algorithm suggested in [4] works based on Voronoi construction and its dual-Delaunay triangulation. All Delaunay based approaches can be put under a single formalism, namely the restricted Delaunay complex, as shown in [10]. Every approach is similar in construction and differs only by how it restricts the Delaunay complex. The CRUST [4] and further improvements Nearest Neighbor-CRUST [8] can handle smooth curves. In [8] small change in the algorithm is done to take care of the reconstruction of curves in $\mathbb{R}^n$, n-dimensional Euclidean space, even with boundaries. The CRUST and NN-CRUST assume that the sample $\mathcal{S}$ is derived from a smooth curve $\mathcal{C}$. The question of reconstructing non smooth curves has also been studied. An extensive experimentation with various curve reconstruction algorithms is carried out in [3]. In [9] an extension of NN-CRUST to $\mathbb{R}^d$ is presented, which opens up possibilities of extending the existing Delaunay based reconstruction algorithms to higher dimensional Euclidean spaces. We will show an example of a curve in $SE(2)$ reconstructed by NN-CRUST.

2.1 Organization of the Article

In this article, we pose the problem of curve reconstruction in higher dimensional curved spaces. We pose the problem as follows. Let $\mathcal{M}$ be a Riemannian manifold and $\mathcal{C} : [0, 1] \to \mathcal{M}$ be a smooth, closed and simple curve. Given a finite sample $\mathcal{S} \subset \mathcal{C}$ reconstruct $\mathcal{C}$. Problem involves defining the appropriate $\mathcal{S}$, suggesting a provable algorithm for geodesic polygonal approximation and an interpolation scheme.

To deal with samples on curved spaces, we will first examine the notion of distance on surfaces and then we will move on to define distances on more general manifolds in

Sect. 3. We equip Riemannian manifold with a metric with the help of a Riemannian inner product. Next we examine the metric structure of $SE(2)$ and $SE(3)$. In Sect. 4 we show with the help of an example that the medial axis based sampling criterion becomes meaningless in curved spaces. Next we define a dense sample set of a smooth curve on Riemannian manifolds. In Sect. 5, we show that it is possible to re-order a dense sample of a curve. We present successfully reconstructed curves in $SE(2)$ and $SE(3)$ in Sect. 6. And finally we conclude in Sect. 7.

3 Metric Structure on Riemannian Manifolds

3.1 $\mathbb{R}^n$ and a Surface in $\mathbb{R}^3$

A curve[1] in space and a curve on surface are two different entities. $\mathbb{R}^n$ can be thought of as a Riemannian manifold with the usual *vector inner product* as the Riemannian metric. The tangent space at a point of $\mathbb{R}^n$ is also an n-dimensional vector space. With the help of the vector inner product, the length of the curve $x : [0, 1] \to \mathbb{R}^n$ is defined as: $L(x) = \int_0^1 \sqrt{\langle x'(t), x'(t)\rangle}\, dt$. It turns out that the minimum length curve between two points in the Euclidean space is a straight line segment connecting them. So the distance between two points in $\mathbb{R}^n$ is given by $d(x, y) = \sqrt{\sum_{i=1}^n (x_i - y_i)^2}$. With this as a metric, $(\mathbb{R}^n, d)$ is a metric space.

Now let us look at a two dimensional surface $\mathcal{M}$ embedded in $\mathbb{R}^3$. Two dimensions here indicate that each point $p \in \mathcal{M}$ has a neighborhood *homeomorphic*[2] to a subset of $\mathbb{R}^2$. In other words, if we associate with each point $p \in \mathcal{M}$ a tangent space $T_p\mathcal{M}$ then the dimension of $T_p\mathcal{M}$ is two,[3] i.e. two linearly independent vectors are required to span $T_p\mathcal{M}$. It is now this tangent space and the basis vectors of this space that decide the Riemannian metric for a given surface. Let us consider a surface patch $x(u, v) \subset \mathbb{R}^3$ parametrized by $(u, v) \in \mathcal{U} \subset \mathbb{R}^2$. In this case x is our manifold $\mathcal{M}$. Riemannian metric is defined as:

$$g_{ij} = \begin{bmatrix} E = \langle x_u, x_u\rangle & F = \langle x_u, x_v\rangle \\ F = \langle x_v, x_u\rangle & G = \langle x_v, x_v\rangle \end{bmatrix} \tag{1}$$

where x_u and x_v are partial derivatives of $x(u, v)$ w.r.t. u and v respectively. Any vector in $T_p\mathcal{M}$ can be expressed in terms of these basis vectors x_u and x_v. The inner product for vectors $x_1, x_2 \in T_p\mathcal{M}$ is given by $\langle x_1, x_2\rangle_g = x_1^T g_{ij} x_2$,

[1] We restrict out attention to smooth curves, i.e. curves which are C^∞.

[2] Homeomorphic here can be replaced by *diffeomorphic* for a differentiable manifold.

[3] For notations and definitions of basic differential geometric terms, we refer to [12].

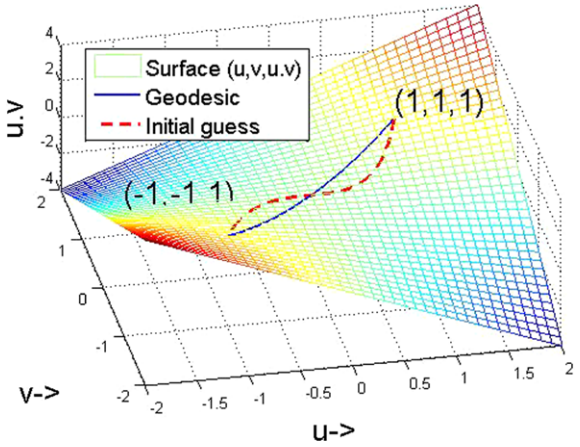

Fig. 1 A bilinear surface and a geodesic

where x_1 and x_2 are column vectors. Given a curve $\gamma(t) \in \mathcal{M}$, the length of curve γ is defined as:

$$L(\gamma) = \int_0^1 \sqrt{\langle \gamma'(t), \gamma'(t)\rangle_g}\, dt \tag{2}$$

Given $p, q \in \mathcal{M}$, let γ be a curve lying in $\mathcal{M}$ with p, q as its end points. Then

$$d(p, q) = \inf L(\gamma) \tag{3}$$

is a valid metric on $\mathcal{M}$. A γ^* for which the distance between two points is minimum is called a *geodesic* curve on the manifold $\mathcal{M}$. As we will see in the following example, even for a simple looking parametrized surface finding a closed form expression for the geodesic curve is difficult. In practice, γ^* is obtained by numerical approximations [14].

Example 1 Let $x(u, v) = (u, v, u \cdot v)$ which leads to $x_u = (1, 0, v)$, $x_v = (0, 1, u)$ and $E = 1 + v^2$, $F = u \cdot v$ and $G = 1 + u^2$. A curve in $x(u, v)$ is, $\gamma(t) = x(u(t), v(t)) = (u(t), v(t), u(t) \cdot v(t))$. The length of the curve $\gamma(t)$, $t \in [t_0, t_1]$ is $\int_{t_0}^{t_1} \sqrt{Eu'^2 + 2 \cdot F \cdot u' \cdot v' + Gv'^2}\, dt$, where u' and v' are du/dt and dv/dt respectively.

If we try to minimize the length function by Euler-Lagrange minimization we get for each of the co-ordinates a second order ordinary non-linear differential equation to solve. In this example these equations are:

$$\frac{d^2u}{dt^2} + 2\frac{v}{1 + u^2 + v^2}\frac{du}{dt}\frac{dv}{dt} = 0 \tag{4}$$

$$\frac{d^2v}{dt^2} + 2\frac{u}{1 + u^2 + v^2}\frac{du}{dt}\frac{dv}{dt} = 0 \tag{5}$$

Let the boundary points, the points between which we are trying to find the geodesic distance, be $(1, 1, 1)$ and $(-1, -1, 1)$. We solve the BVP for the above system of equations with MATLAB boundary value solver. The resultant geodesic and the initial guess are shown in Fig. 1.

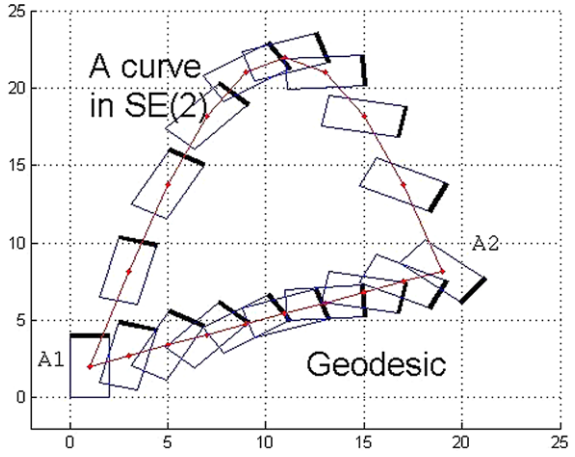

Fig. 2 Comparision of a curve and a geodesic in $SE(2)$ between two configurations A_1 and A_2

3.2 Euclidean Motion Groups

Consider an object in plane undergoing a rigid body Euclidean motion. This motion can be decomposed into a rotation with respect to the center of mass of the object and a translation of the center of mass of the object. All possible configurations of an object in plane can be represented by (θ, u, v) (i.e. orientation of the principle axis and the co-ordinates of the center of mass of the object), where $0 \leq \theta < 2\pi$ and $(u, v) \in \mathbb{R}^2$. Let all such configurations form a set $\mathbb{S}$. It is rather straight forward to define a metric on $\mathbb{S}$ so as to define nearness of two configurations of an object. If $A_1 = (\theta_1, u_1, v_1)$ and $A_2 = (\theta_2, u_2, v_2)$ be two configurations in $\mathbb{S}$ then it is easy to verify that

$$d(A_1, A_2) := \sqrt{a(\theta_1 - \theta_2)^2 + b(u_1 - u_2)^2 + b(v_1 - v_2)^2} \tag{6}$$

is a valid metric on $\mathbb{S}$ corresponding to the Riemannian inner product $\langle A_1, A_1 \rangle_R = A_1^T R A_1$, and $R = \left[\begin{smallmatrix} a & 0 \\ 0 & bI_2 \end{smallmatrix}\right]$ a positive definite matrix. Moreover, for given A_1 and A_2, left composition with $A \in \mathbb{S}$, i.e. $A(A_1) = (\theta + \theta_1, u + u_1, v + v_1)$, the above defined metric leads to $d(A_1, A_2) = d(A(A_1), A(A_2))$. Hence we have a left invariant metric defined on $\mathbb{S}$. Physical interpretation of the left invariance is, the freedom in choice of inertial reference frame. A typical curve between two configurations in $SE(2)$ and the geodesic segment from A_1 to A_2 are shown in Fig. 2.

Similarly, consider a rigid body moving in free space. We fix an inertial reference frame $\{B\}$ at the origin O and a frame $\{E\}$ to the body at some point O' of the body as shown in Fig. 3. At each instance the configuration of the rigid body is described via a transformation matrix, $A \in SE(3)$, corresponding to the displacement from frame $\{B\}$ to frame $\{E\}$.

So a rigid body motion becomes a curve in $SE(3)$, let $A(t)$ be such a curve given by $A(t) : [-c, c] \to SE(3)$,

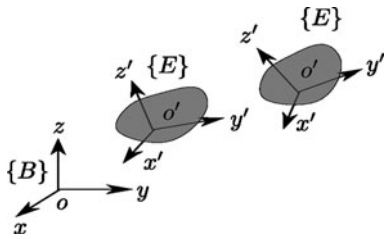

Fig. 3 Inertial frame $\{B\}$ and body fixed frames $\{E\}$

$A(t) = \left[\begin{smallmatrix} R(t) & d(t) \\ 0 & 1 \end{smallmatrix}\right]$, where $R \in SO(3)$, a rotation matrix, and $d \in \mathbb{R}^3$ is a displacement vector. The lie algebra element $S(t) \in se(3)$ can be identified with the tangent vector $A'(t)$ at any t by:

$$S(t) = A^{-1}(t)A'(t) = \begin{bmatrix} [\omega](t) & v(t) \\ 0 & 0 \end{bmatrix} \tag{7}$$

where $[\omega]$ is a skew symmetric matrix [12] corresponding to the vector $\omega = [\omega_x\ \omega_y\ \omega_z] \in \mathbb{R}^3$. $\omega = [\omega_x, \omega_y, \omega_z] \in \mathbb{R}^3$. The $\|\omega\|$, $\|\cdot\|$ represents the standard Euclidean norm, gives the amount of rotation with respect to the unit vector along ω. The exponential map exp, is a diffeomorphism [25] connecting Lie algebra to corresponding Lie group. The $\exp : se(3) \to SE(3)$ is given by the usual matrix exponential as $\exp(S) = \sum_{n=0}^{\infty} \frac{S^n}{n!}$. The ω physically corresponds to the angular velocity of the body, while v is the linear velocity of the origin O'.

Let us assign a Riemannian metric $g = \left[\begin{smallmatrix} \alpha I_3 & 0 \\ 0 & \beta I_3 \end{smallmatrix}\right]$ over $SE(3)$ as prescribed in [20]. And so for $V = (\omega, v) \in se(3)$, $\langle V, V \rangle_g = \alpha\omega^T\omega + \beta v^T v$. It is proved in [25] that the analytic expression for the geodesic between two configurations A_1 and A_2 in $SE(3)$, with g as Riemannian metric, is given by

$$R(t) = R_1 \exp\big([\omega_0]t\big) \tag{8}$$

$$d(t) = (d_2 - d_1)t + d_1 \tag{9}$$

where $[\omega_0] = \log(R_1^T R_2)$ and $t \in [0, 1]$. The path is unique for $\text{Trace}(R_1^T R_2) \neq -1$. And the distance between two configuration in $SE(3)$ is given by

$$d(A_1, A_2) = \sqrt{\alpha \big\| \log\big(R_1^{-1} R_2\big) \big\|^2 + \beta \|d_2 - d_1\|^2}. \tag{10}$$

All the formulas required for computing exp and log maps are given in the Appendix for completeness.

Example 2 Consider two configurations A_1 and A_2, as shown in Fig. 4, given by vectors (ω_1, v_1) and (ω_2, v_2) respectively, where $\omega_1 = \frac{\pi}{4}[1\,0\,0]$, $v_1 = [-6\,0\,0]$, $\omega_2 = \frac{\pi}{2}[1\,1\,0]$ and $v_2 = [0\,6\,2]$.

Once a particular Riemannian metric is identified, we can construct a distance metric on the manifold. With the distance metric $d(\cdot, \cdot)$ (corresponding to the length of a geodesic path) defined on Riemannian manifold, we are now

ready to discuss about the medial axis and the sampling criterion for a curve on the given manifold.

4 Medial Axis, Dense Sample

We proceed by revisiting the definition of medial axis stated previously. Let $\mathcal{M}$ be a Riemannian manifold and $d(\cdot,\cdot) : \mathcal{M} \times \mathcal{M} \to \mathbb{R}$ be the corresponding distance metric.

Definition 1 The medial axis M of a curve $\mathcal{C} \subset \mathcal{M}$, is the closure of set of points in $\mathcal{M}$ that have at least two closest points in $\mathcal{C}$.

Figure 5 shows examples of medial axis of closed curves on a half cylinder and in a plane. It should be noted here that the medial axis, as defined above, is a subset of the underlying manifold in which the curve lies. A curve embedded in a general Riemannian manifold and embedded in $\mathbb{R}^3$ will have different medial axes. The open disc (ball) of radius $\varepsilon > 0$ in $\mathcal{M}$ with $s \in \mathcal{M}$ as a center is defined as $S_\varepsilon(s) = \{x \in \mathcal{M} | d(s,x) < \varepsilon\}$. In the same manner $B_\varepsilon(s) = \{x \in \mathcal{M} | d(s,x) \leq \varepsilon\}$ is a closed disc (ball) in $\mathcal{M}$ with radius ε and the center s. The set $\partial B_\varepsilon(s) = \{x \in \mathcal{M} | d(x,s) = \varepsilon\}$ is the boundary of $B_\varepsilon(s)$.

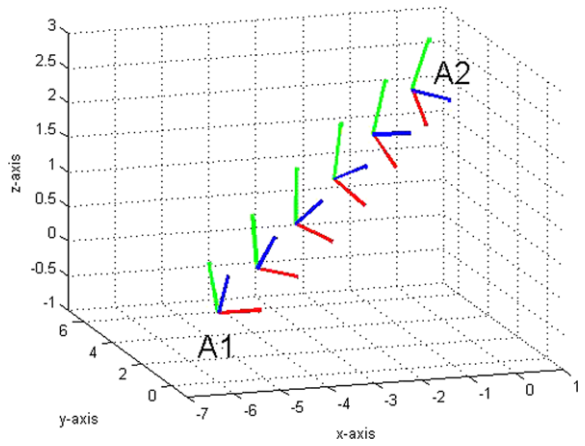

Fig. 4 A geodesic between $A_1, A_2 \in SE(3)$

Definition 2 At a point p on curve $\mathcal{C}$ the local feature size $f(p) = d(p, M)$. Where $d(p, M) = \inf\{d(p,m), \forall m \in M\}$ and M is the medial axis of $\mathcal{C}$.

The local feature size at a point on a curve captures the behavior of that curve in the neighborhood of given point. In practice for arbitrary curves it is difficult to identify the medial axis. Looking at the construction of the *Voronoi* diagram [19], for a given sample points of a curve the Voronoi vertices do capture the behavior of the medial axis of the sampled curve. And so for a densely sampled curve the Voronoi vertices for these samples are taken to be the approximate of the medial axis of the given curve. It is computationally challenging to construct Voronoi diagrams on curved spaces [15].

4.1 Dense Sampling

A tubular neighborhood for a curve in a plane is defined as the subset of the plane such that every point of the subset belongs to exactly one line segment totally contained in the subset and normal to the curve. A disk centered at a point of a curve contained in a tubular neighborhood of that curve is called a tubular disk. Let us generalize this definition to curves in manifolds. We will also define the notion of a dense sample of a curve in manifold based on its tubular neighborhood.

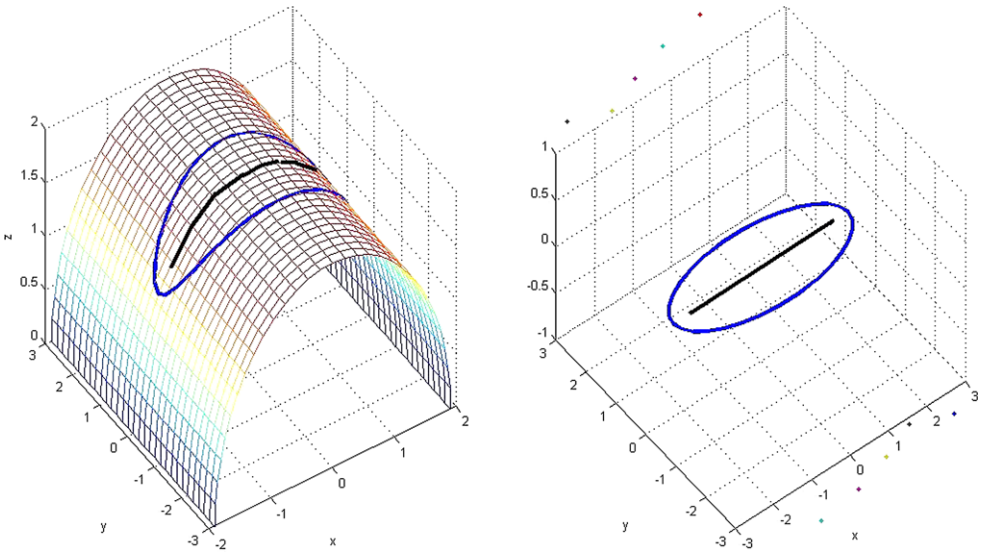

Fig. 5 Medial axis of a curve on a surface and a curve in a plane

Definition 3 Let $\mathcal{C} \subset \mathcal{M}$ be a smooth curve. Consider segments of geodesics that are normal to $\mathcal{C}$ and start in $\mathcal{C}$. If $\mathcal{C}$ is compact, then there exists an $\varepsilon > 0$ such that no two segments of length ε and starting at different points of $\mathcal{C}$ intersect [23]. The union of all such segments of length ε is an open neighborhood T of $\mathcal{C}$, and is called a tubular neighborhood of $\mathcal{C}$.

We denote the open segment with center $p \in \mathcal{C}$ and radius ε in the normal geodesic segment of $\mathcal{C}$ at p by $N_\varepsilon(p)$. Revisiting the definition of the tubular neighborhood: the union $N_\varepsilon(\mathcal{C}) = \bigcup_{p\in\mathcal{C}} N_\varepsilon(p)$ is called a tubular neighborhood of radius ε if it is open as a subset of $\mathcal{M}$ and the map $F : \mathcal{C} \times (-\varepsilon, \varepsilon) \to N_\varepsilon(\mathcal{C})$ is a diffeomorphism. This interpretation is the outcome of result from [7]. Let $\mathcal{C} \subset \mathbb{R}^2$, be a simple closed smooth curve. Existence of the tubular neighborhood is evident from the compactness of the curve in $\mathbb{R}^2$. We show something more about the value of ε in the next proposition.

Proposition 1 *If $N_\varepsilon(\mathcal{C})$ is a tubular neighborhood of $\mathcal{C}$ then $\varepsilon < \frac{1}{k}$. Where $k = \max k(p)$, $p \in \mathcal{C}$ and $k(p)$ is the curvature of the curve at point p.*

Proof Let us define a curve $\alpha(s)$ in $\mathbb{R}^2$ by

$$\alpha(s) = F\big(\mathcal{C}(s), t\big) = \mathcal{C}(s) + tN\big(\mathcal{C}(s)\big),$$

for a fixed $t \in (-\varepsilon, \varepsilon)$ such that at $t = 0$, $\alpha(0) = p$. $N(p)$ is the unit normal to the curve $\mathcal{C}$ at p. This new curve belongs to the open set $N_\varepsilon(\mathcal{C})$ and

$$\alpha(0) = p + tN(p) \tag{11}$$

$$\alpha'(0) = \mathcal{C}'(0) + tN'(0) \tag{12}$$

$$\alpha'(0) = \big(1 - tk(p)\big)\mathcal{C}'(0) = (dF)_{(p,t)}\big(\mathcal{C}'(0)\big). \tag{13}$$

Since $F : \mathcal{C} \times (-\varepsilon, \varepsilon) \to \mathbb{R}^2$ is a diffeomorphism when restricted to $\mathcal{C} \times (-\varepsilon, \varepsilon)$, we have that $(dF)_{(p,t)}(\mathcal{C}'(0))$ is a non-null vector, i.e. $1 - tk(p) \neq 0$. Since $(-\varepsilon, \varepsilon)$ is connected and $1 - tk(p) > 0$ for $t = 0$, so $1 - tk(p) > 0$ on $\mathcal{C} \times (-\varepsilon, \varepsilon)$. Now if $k = \max k(p)$, $p \in \mathcal{C}$ then $1 - tk > 0$. And we have $\varepsilon = t < \frac{1}{k}$. □

Definition 4 A finite sample set $\mathcal{S} \subset \mathcal{C}$ is called a *uniform ε-sample* for some $\varepsilon > 0$ if for any two consecutive sample points $r, s \in \mathcal{S}$, $r \in B_\varepsilon(s)$.

Definition 5 A uniform ε-sample $\mathcal{S}$ of a curve $\mathcal{C} \subset \mathcal{M}$ is dense if there is a real number $\varepsilon > 0$ such that $\bigcup_{s\in\mathcal{S}} B_\varepsilon(s)$ forms a tubular neighborhood of C.

Proposition 2 *For plane curves if $\varepsilon < \min_{p\in\mathcal{C}} f(p)$ then the uniform ε-sample $\mathcal{S}$ of curve $\mathcal{C}$ is a dense sample.*

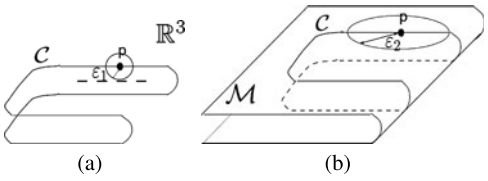

(a) (b)

Fig. 6 (**a**) A curve $\mathcal{C} \in \mathbb{R}^3$ and the part of medial axis near $p \in \mathcal{C}$. ε_1 is the distance of the point $p \in \mathcal{C}$ from the medial axis of the curve in space. (**b**) The same curve $\mathcal{C}$ on a surface $\mathcal{M}$ and the medial axis distance ε_2 from the point $p \in \mathcal{C}$ to the medial axis of the curve on the surface

Proof By the definition of $f(p)$, $p \in \mathcal{C}$, for a smooth curve $\mathcal{C}$, the $f(\cdot)$ attains maximum value at the points where the curvature of $\mathcal{C}$ is maximum. For the $\varepsilon < \min_{p\in\mathcal{C}} f(p)$, let the uniform ε-sample be $\mathcal{S} \subset \mathcal{C}$. From Proposition 1, we see that $\forall s \in \mathcal{S}$, $\bigcup_{s\in\mathcal{S}} B_\varepsilon(s)$ covers the curve $\mathcal{C}$ and is a tubular neighborhood of $\mathcal{C}$. So, $\mathcal{S}$ is dense. □

Before we proceed to the main theorem we will discuss a few observations in next section. We show by an example how the medial axis based sampling fails due to the curvature of the underlying Riemannian manifold. We also propose to work within the injectivity radius of manifold to avoid such a problem. Observations presented in next section suggest that the additional knowledge of the manifold on which the curve is lying allows for a sparser sampling densities. A counter example to the medial axis based sampling presented in the next section will help us in identifying a conservative sampling criterion for curves.

4.2 Observations and a Counter Example

We know that to form a dense sample of a curve in $\mathbb{R}^n$ it is required to sample with the $\varepsilon_1 < \min_{p\in\mathcal{C}} f(p)$. A curve and the corresponding ε_1 is shown in Fig. 6(a). Whereas if the same curve is embedded in a surface, as shown Fig. 6(b), the required ε_2 will depend upon the nature of the surface. It turns out that $\varepsilon_2 > \varepsilon_1$. Let us look at another example. A circle in the xy-plane in $\mathbb{R}^3$ can be thought of as some latitude on a sphere of radius $r \geq \frac{L}{2\pi}$, where L is the length of the circle. In both the cases, circle on a plane and circle on a sphere, the sampling required for correct reconstruction is different. On sphere we need less dense sample set as compared to the plane. In fact as we increase the radius r we need denser and denser sample set for correct reconstruction and its limiting case, $r \to \infty$, is the plane. In $\mathbb{R}^3$ the usual Euclidean metric is carried over to the points of the circle. In case of sphere the shortest path between two points is always along the great circle passing through these two points. And the length of the segment which is shorter is the distance between two points on sphere. With this metric defined, sphere becomes a metric space. And the points of the circle on sphere are endowed with this metric. The points

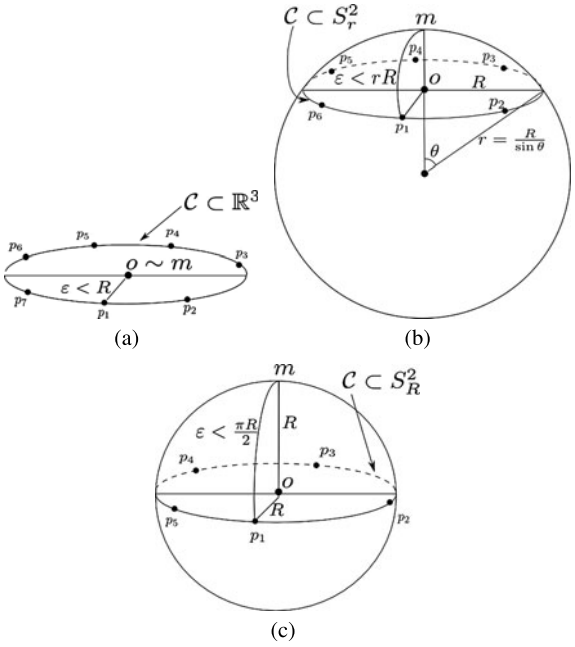

Fig. 7 (**a**) Circle with radius R is lying in space. (**b**) Circle resting on a sphere of radius $r = \frac{R}{\sin\theta}$. (**c**) Circle is the great circle the sphere of radius R

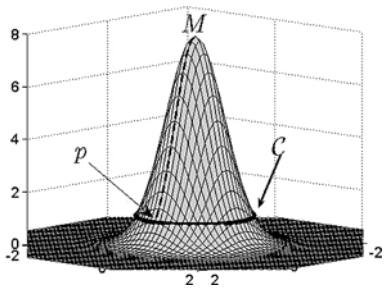

Fig. 8 A circle $\mathcal{C}$ and the normal geodesic from a point $(1, 0, 1.0629)$ to M

of this circle on a sphere are more structured then the points of the same circle in $\mathbb{R}^3$. The additional knowledge of the underlying surface adds up to the ordering relation between points of the circle. Since we know the surface we know the tangent space and that reduces the effort in ordering the sample points.

Interestingly, when generalized to the curves on manifolds, the sampling criterion based only on the medial axis becomes meaningless. As an example let us look at a circle of radius one on the surface shown in Fig. 8. The medial axis of the circle on the given surface is the point $M(0, 0)$, where the surface M is parametrized as $M(u, v) = 7.85e^{-2(u^2+v^2)}$. For any point on the circle, the distance from the medial axis turns out to be larger than the length of the circle itself. Consider the limiting case of this surface, a cylinder, suppose the circle is on the cylinder. The medial axis point does not exist.

The above phenomenon can be understood clearly if we look at the cut locus of the point $p \in \mathcal{M}$. Following can be considered as the defining property of the cut locus of a point on the manifold. If $\gamma(t_0)$ is the cut point of $p = \gamma(0)$ along the geodesic arc γ then either $\gamma(t_0)$ is the first conjugate point of $\gamma(t_0)$ or there exists a geodesic $\sigma = \gamma$ from p to $\gamma(t_0)$ such that $l(\sigma) = l(\gamma)$ (lengths of σ and γ are equal).

For example if $\mathcal{M}$ is a sphere S^2 and $p \in S^2$ then the cut locus of p is its antipodal point. And if we consider the sphere of radius R the distance of point p from its cut locus is πR. Whereas the distance of the points p_i on the circle in Fig. 7(c) to the medial axis M is $\frac{\pi R}{2}$. Now coming back to the counter example in Fig. 8 we observe that the distance of the point p to its cut locus $d(p, C_m(p))$, where $C_m(p)$ is the cut locus of $p \in \mathcal{M}$, is less then the distance to the medial axis M of the circle. It can be shown that if $q \in \mathcal{M} - C_m(p)$ there exists a unique minimizing geodesic joining p and q. In [7]

$$i(\mathcal{M}) = \inf_{p \in \mathcal{M}} d\big(p, C_m(p)\big) \tag{14}$$

is defined as the injectivity radius of $\mathcal{M}$. So if $\varepsilon < i(\mathcal{M})$ then $\exp_p$ is injective on the open ball $S_\varepsilon(p)$.

Tubular neighborhood of a curve is constructed by taking only the normal geodesics to the curve at a point and assuring the injectivity of the $\exp_p$ map along these normal directions. Now, we propose to work inside the injectivity radius to resolve the problem with sampling.

Proposition 3 *Let $\mathcal{C} \in \mathcal{M}$ be a smooth, simple and closed curve. If $\mathcal{S}$ is a uniform ε-sample of $\mathcal{C}$ then $\mathcal{S}$ is dense for $\varepsilon < \min\{\inf_{p \in \mathcal{C}} f(p), i(\mathcal{M})\}$.*

Proof Let $\mathcal{S}$ be a uniform ε-sample of $\mathcal{C}$ with $\varepsilon < \min\{\inf_{p \in \mathcal{C}} f(p), i(\mathcal{M})\}$. From the definitions of the injectivity radius and the feature size we know that for the above mentioned ε, $\exp_p$ is injective on $S_\varepsilon(p)$. So, $\bigcup_{s \in \mathcal{S}} B_\varepsilon(s)$ forms a tubular neighborhood of $\mathcal{C}$. And hence $\mathcal{S}$ is dense. □

4.3 Behavior of a Curve Segment Inside a Tubular Neighborhood

If the underlying manifold is a plane and the sample of a curve is dense enough then based on the tubular neighborhood it is shown in [11] that Euclidean minimal spanning tree reconstructs the sampled arc. The crucial argument for the correctness of above is the denseness of the sample. The argument rests on the observation that an arc does not wander too much inside a tubular disk. This behavior of the curve segment avoids the connections between the non-consecutive sample points in $\mathcal{S}$, defined as short chords.

Next we give an alternate proof of flatness of the curve segment inside a tubular neighborhood in plane, then go on to extend the proof to curves in the Riemannian manifold.

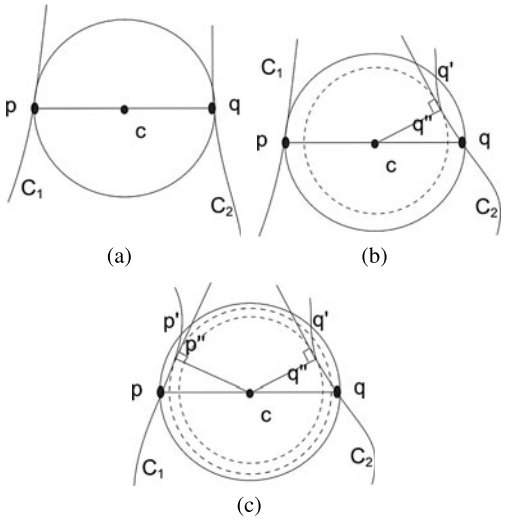

Fig. 9 (**a**) The arc touches $B_{pq/2}(c)$. (**b**) The arc touches $B_{pq/2}(c)$ at p and intersects its boundary at q' while passing through q. (**c**) The arc intersects boundary of $B_{pq/2}(c)$ at p' and q' while passing through p and q respectively

Theorem 1 *Let p and q be two points on an arc $\mathcal{C} \subset \mathbb{R}^2$ such that q is inside the tubular disk $B_\varepsilon(p)$ centered at p. Then the sub arc pq of $\mathcal{C}$ is completely inside $B_{pq/2}(c)$, where c is the center of diameter pq.*

Proof Since $q \in B_\varepsilon(p)$, $pq = d(p,q) \leq \varepsilon$. Now pq being a segment of an arc $\mathcal{C}$ there are three possible ways, as shown in Fig. 9, in which it can intersect with $B_{pq/2}(c)$.

For the possibility shown in Fig. 9(a), it is evident that center c lies on two normals passing through p and q, i.e. $c \in \overline{pq}$, since $B_{pq/2}(c)$ and $\mathcal{C}$ share common tangents at p and q. This can not happen since $B_{pq/2}(c) \subset B_\varepsilon(p)$, a subset of a tubular neighborhood.

Let us consider the case in Fig. 9(b), arc $\mathcal{C}$ touches $B_{pq/2}(c)$ at p and intersects the boundary of $B_{pq/2}(c)$ at q and q'. We can find out a point q'' on the segment qq' which is nearest to c. At q'' the circle with center c and radius $d(c,q'')$ shares a common tangent with $\mathcal{C}$. Hence c lies on the two normals $\overline{pc}$ and $\overline{q''c}$. This can not happen inside a tubular neighborhood.

Finally we consider Fig. 9(c). On segments pp' and qq' we find p'' and q'' nearest to c. In this case c lies on $\overline{p''c}$ and $\overline{q''c}$. Since c is inside tubular neighborhood this can not happen.

So the only possibility we are left with is that the segment pq of curve $\mathcal{C}$ lies entirely inside $B_{pq/2}(c)$. □

Theorem 2 *Let p and q be two points on an arc $\mathcal{C} \subset \mathcal{M}$, where $\mathcal{M}$ is any Riemannian manifold, such that q is inside the tubular disk $B_\varepsilon(p)$ centered at p. Then the sub arc pq of $\mathcal{C}$ is completely inside $B_{pq/2}(c)$, where c is the center of diameter pq.*

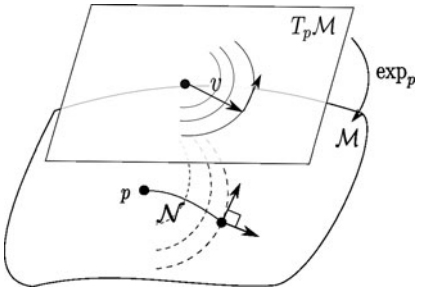

Fig. 10 Tangent space of a point $p \in \mathcal{M}$ where $\|v\| < \varepsilon$ and the corresponding geodesic $\mathcal{N}$

Proof For $\mathcal{M} := \mathbb{R}^n$ we know that $\overline{cp}$, since $p \in S^{n-1}$, is orthogonal to T_pS^{n-1}. S^{n-1} is a unit sphere in $\mathbb{R}^n$.

Since we are working inside a tubular neighborhood of the curve $\mathcal{C}$, with ε as prescribed in Proposition 3, $\exp : T_p\mathcal{M} \to \mathcal{M}$ is a diffeomorphism. Gauss's lemma [7] asserts that the image of a sphere of sufficiently small radius ($< \varepsilon$) in $T_p\mathcal{M}$ under the exponential map is perpendicular to all the geodesics originating at p, see Fig. 10.

The rest of the proof follows from the arguments stated in the proof of Theorem 1. □

5 Curve Reconstruction on a Riemannian Manifold

5.1 Ordering

We model a curve with a graph where the vertices of the graph are the sample points and the edges indicate the order in which the vertices are connected. This also implies a geometric realization of the graph. If further we put the distance between two sample points as the edge cost, it becomes a weighted graph. A minimal spanning tree for a weighted graph is a spanning tree for which the sum of edge weights is minimal. To keep the notations consistent we define the geodesic polygonal path on Riemannian manifold as the path along which every vertex (sample point) pair is connected by a geodesic segment.

Computing the minimal spanning tree (MST) uses the following fundamental property, let $X \cup Y$ be a partition of the set of vertices of a connected weighted graph G. Then any shortest edge in G connecting a vertex of X and a vertex of Y is an edge of a minimal spanning tree. If we use MST to model an arc, we must ensure that there are no short chords in the graph, as proved in [11].

Our work focuses on closed, simple, smooth curves. The sample points will exactly two neighbors (samples) on the curve, thereby giving an MST in which every vertex has degree 2.

Theorem 3 *If $\mathcal{S}$ is a dense sample of $\mathcal{C} \subset \mathcal{M}$ then MST gives a correct geodesic polygonal reconstruction of $\mathcal{S}$, where $\mathcal{C}$ is a smooth, closed and simple curve.*

Proof We show that the geodesic polygonal path has no short chords. The argument is similar to the proof provided for planar case in [11]. For the completeness of the article we restate the argument here. Suppose that MST does not give a correct geodesic polygonal reconstruction of $\mathcal{S}$. It implies that there are at least two points in MST which are not consecutive. Let these points be $p, q \in \mathcal{S}$. Since pq is a short chord there has to be at least one edge in the sub arc pq which has length greater than that of pq. But since the sample $\mathcal{S}$ is dense, the arc pq must be contained in the disc with diameter pq. Inside the disc there is no arc with length greater than the length of the diameter. So we have a contradiction. □

5.2 Interpolation

Once we have ordered the given set of points of the curve on a curved manifold the next step is to interpolate this point set to the desirable granularity. The easiest way to interpolate the points is to connect the points via straight line segments, a linear interpolation. In general for a manifold like $SE(3)$, the geodesics are the exp segments. But this scheme will not produce a differentiable curve which might be necessary for some applications. Based on the need and application one may chose an appropriate interpolation scheme. In [22] and [13] a quaternion based approach is suggested and is very useful in computer graphics and animation. Since we have represented $SE(3)$ using matrices we would rather stick to matrices. Motivated by motion planning purposes various interpolation schemes based on variational minimization techniques have been proposed and some of them turn out to be quite simple for implementations. For a broad overview one will find [21] and [16] useful. As the final stage in the reconstruction we have used *de Casteljau* interpolation scheme as prescribed in [1], i.e. generalizing the multilinear interpolation on $SE(3)$, a piecewise C^2 curve connecting two frames with given velocities. The advantage is that the expression is in the closed form with exponential and log maps. Suppose that we do not know the velocities at the node points. For such cases we have used a partial geodesic scheme to interpolate between two elements of $SE(3)$. Wherein, the rotational part is interpolated by the exp map and the translational component is interpolated by spline segments. With the help of an example, a comparison between both the interpolation schemes is shown in Fig. 11. A descriptive summary of the curve reconstruction algorithm is given next.

5.3 Summary of Algorithm

We begin with a set $\mathcal{S} := \{s_0, s_1, \ldots, s_{n-1}\}$ of sample points of the curve $\mathcal{C} \subset \mathcal{M}$. We assume that $\mathcal{S}$ is a dense sample. Using the Riemannian metric defined on $\mathcal{M}$ we calculate distances, $d(s_i, s_j), i \neq j$, between sample points

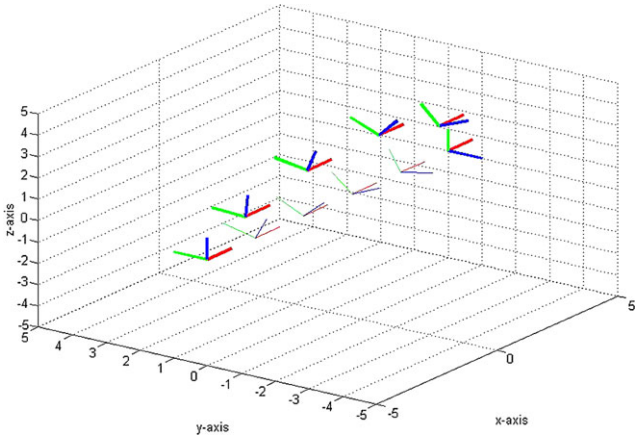

Fig. 11 Comparision of exponential map and C^2 smooth interpolation in $SE(3)$ between $g_0 = [0, 0, 0] \ltimes [-5, 0, 0]$ and $g_1 = [\pi/2, 0, 0] \ltimes [5, 0, 0]$, with tangents $v_0^1 = [0, 0, 0, 3, 1, 1]$ and $v_2^1 = [\pi/2, 0, 0, -1, -3, -1]$

for $i, j = 1, 2, \ldots, n-1$. Using the minimum spanning tree algorithm we reorder the set of sample points. $\mathcal{S}_\sigma = \{s_{\sigma(0)}, s_{\sigma(1)}, \ldots, s_{\sigma(n-1)}\}$ is the reordered set where σ is a permutation on the set of n symbols. We interpolate $\mathcal{S}_\sigma$ using the de Casteljau interpolation scheme and produce a C^2 continuous curve.

6 Simulations

6.1 Curves on a Sphere

We start with examples of curves on a unit sphere. We show two curves with different densities required by the MST for correct reordering of the samples in Fig. 12.

The curves after reordering the sample points are shown in Figs. 12(a) and 12(b).

6.2 Curves in $SE(3)$

In Fig. 13 an unordered set of frames in $SE(3)$ are shown. We assume that the sample shown is dense.

By the distance metric defined in (10) we compute distances between all the frames. We then compute the MST for the complete weighted graph of frames with the computed distances as the edge weights.

Once the ordering is done we interpolate the sample with partial geodesic scheme. Results of interpolation with two different granularities is presented in Figs. 14 and 15.

6.3 Another Useful Manifold : $SE(2)$ with Scaling

Suppose for a planar object in motion, we include scaling with respect to the center of mass along with rotation and

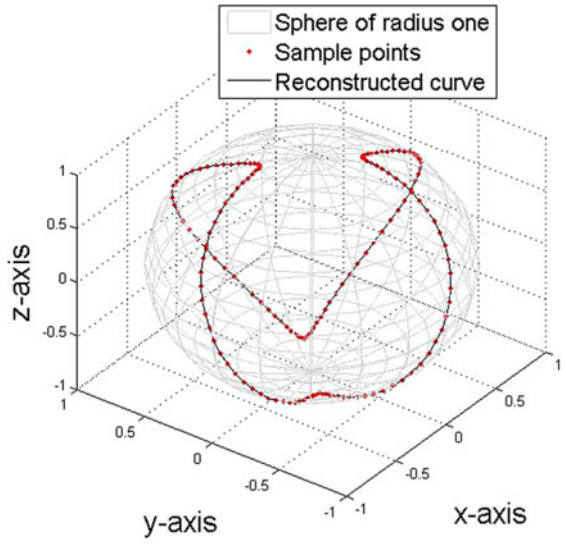

(a)

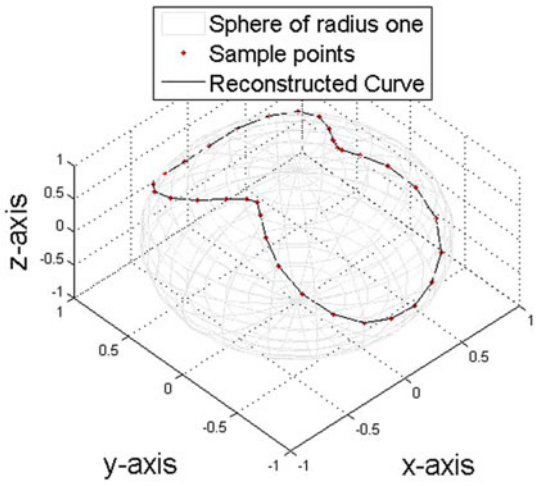

(b)

Fig. 12 Example curves on a unit sphere

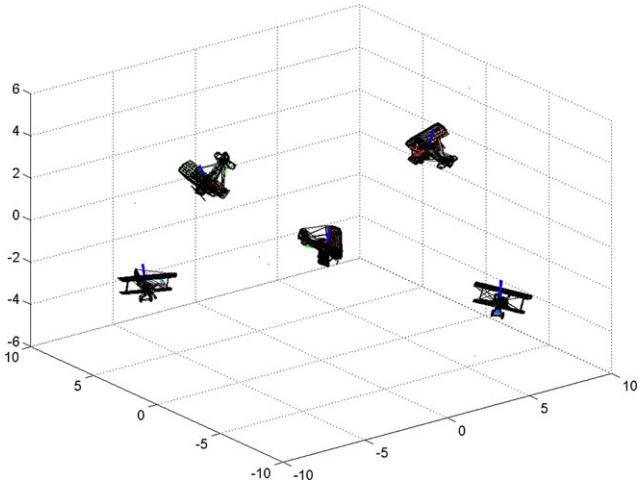

Fig. 13 A sample $\mathcal{S}$ of a curve $\mathcal{C} \subset SE(3)$

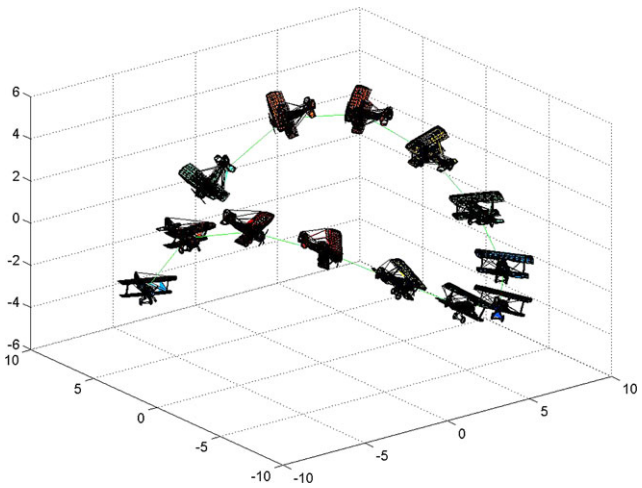

Fig. 14 Reconstructed curve in $SE(3)$

translation. The resultant element will be of the following form

$$A = \begin{bmatrix} e^{\lambda} R & d \\ 0 & 1 \end{bmatrix} \in \mathbb{R}^3. \tag{15}$$

This element operates on the point of the object in plane. It scales (e^{λ}) and rotates (R) the object with respect to its center of mass and then translates (d) the center of mass. With each such element we can associate a vector $[\lambda, \theta, d_x, d_y]$. The elements of the form given by (15) with standard matrix multiplication forms a lie group. We can extend the notions of tangent space and exponential map to this lie group. As discussed previously in Sect. 3.2 this group is a semi-direct product of elements of scaled rotations and translations. The tangent space elements at identity, lie algebra elements, for scaled rotations are given by

$$[a] = \lambda \begin{bmatrix} 1 & 0 \\ 0 & 1 \end{bmatrix} + \theta \begin{bmatrix} 0 & -1 \\ 1 & 0 \end{bmatrix}. \tag{16}$$

And the usual matrix exponentiation gives

$$\exp[a] = e^{\lambda} \begin{bmatrix} \cos\theta & -\sin\theta \\ \sin\theta & \cos\theta \end{bmatrix}. \tag{17}$$

We can construct a left-invariant Riemannian metric on this group. It can be shown that for two elements A_1, A_2 in this group

$$d(A_1, A_2) = \sqrt{\alpha\big((\lambda_1 - \lambda_2)^2 + (\theta_1 - \theta_2)^2\big) + \beta \|d_1 - d_2\|} \tag{18}$$

is a valid distance metric. In Fig. 16, a circular object under the action of this group is shown for various time steps. Assuming the curve is sampled densely, along with the distance

measured by (18) we reconstruct the curve using MST. The successfully reconstructed curve, with the values $\alpha = 10$ and $\beta = 1$, is shown in Fig. 17. Important fact to note here is that the curve presented here is not a closed curve. The algorithm is modified in this case to take care of the end points. In fact a simple nearest neighbour search will also do the job of reconstruction once we give in the initial point. The values of α and β depends upon the linear and rotational velocities.

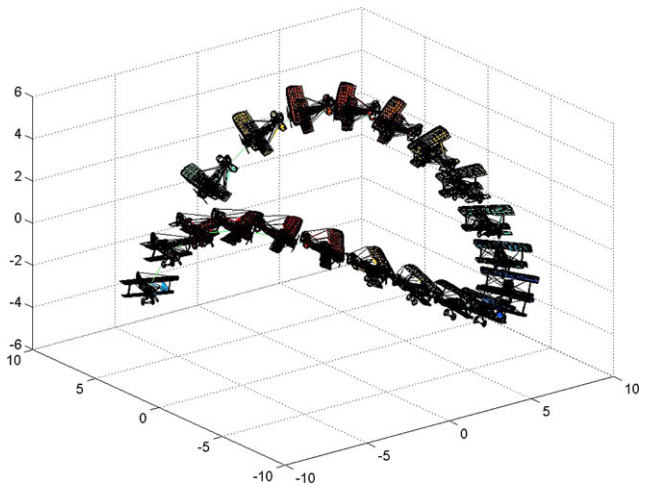

Fig. 15 Reconstructed curve in $SE(3)$ with finer interpolation

Whichever velocity is varying slowly higher weight should be given to that component of the metric.

6.4 Application to Video Frame Sequencing

As an application of the curve reconstruction we take up a task of ordering the frames $\{F_i\}_{i=1,\ldots,N}$ of a video sequence. In Fig. 18 there are sixteen frames of a video sequence. We use the rigid Euclidean motion of an object in the frames as a clue for re-ordering the frames. Let us assume that the object under observation is masked by a rectangle and it is segmented out of the frames. We also assume that the motion of the object is the rigid body Euclidean motion in $\mathbb{R}^2$. Further let the video frames from the sequence form a dense sample set of the motion curve. As discussed in Sect. 3.2 we calculate the distances between frames as the distance between elements of $SE(2)$. Although we do not focus on how to estimate the rotations we give a very primitive looking argument below to estimate the distances between two frames. And it turns out that the estimates are good enough in this case to reconstruct the curve. But in general we use the $[\theta, x, y]$ as the element of $SE(2)$ and we assume that we have an oracle to give these frame coordinates to the algorithm. We have done experiments with template matching based registration algorithm as suggested in [17]. It is used extensively in the domain of computer vision and image processing. It estimates the Euclidean transformations

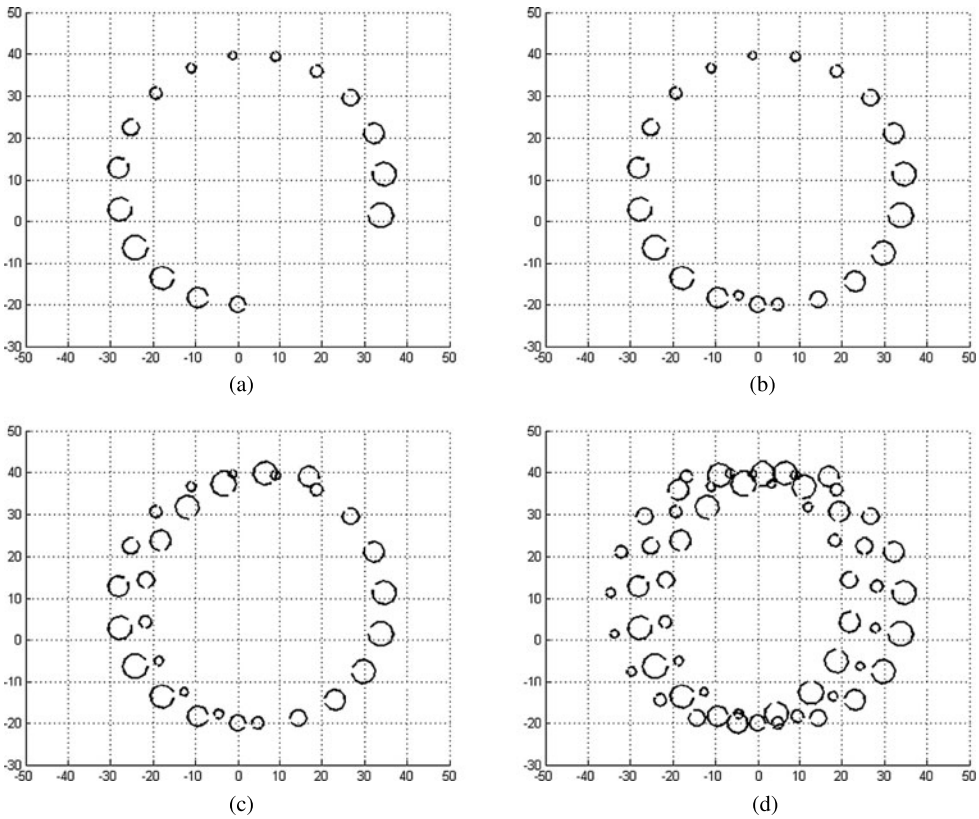

Fig. 16 Various instances of a curve in $SE(2)$ with scaling

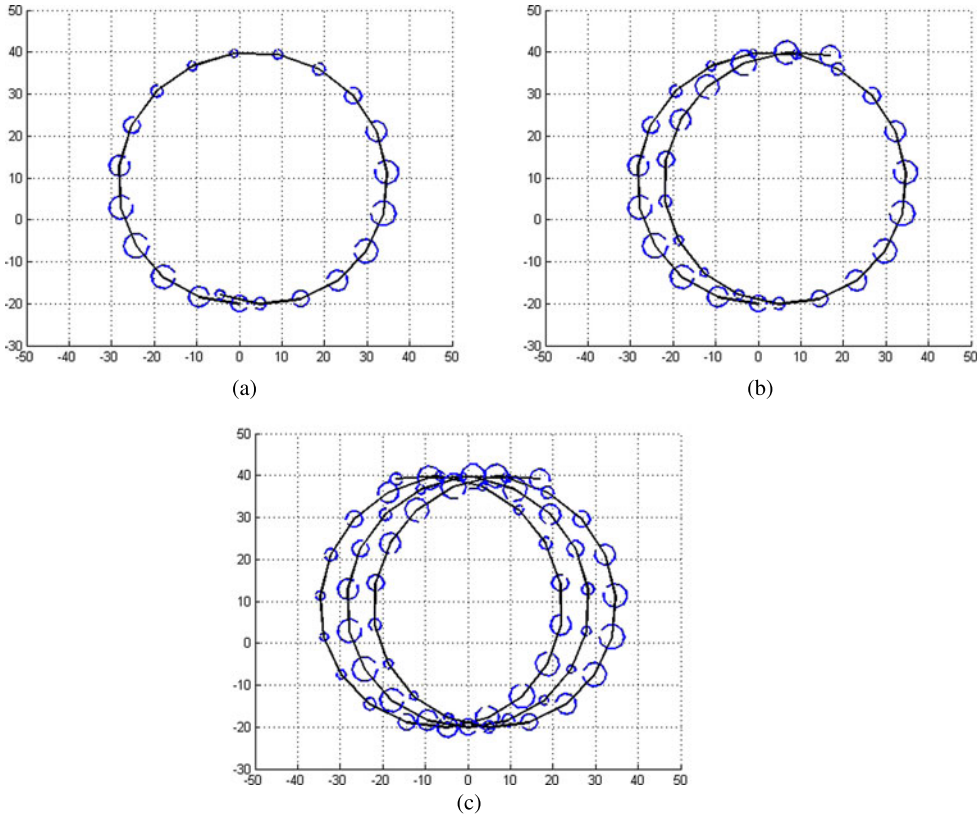

Fig. 17 Instances of the reconstructed curve in $SE(2)$ with scaling

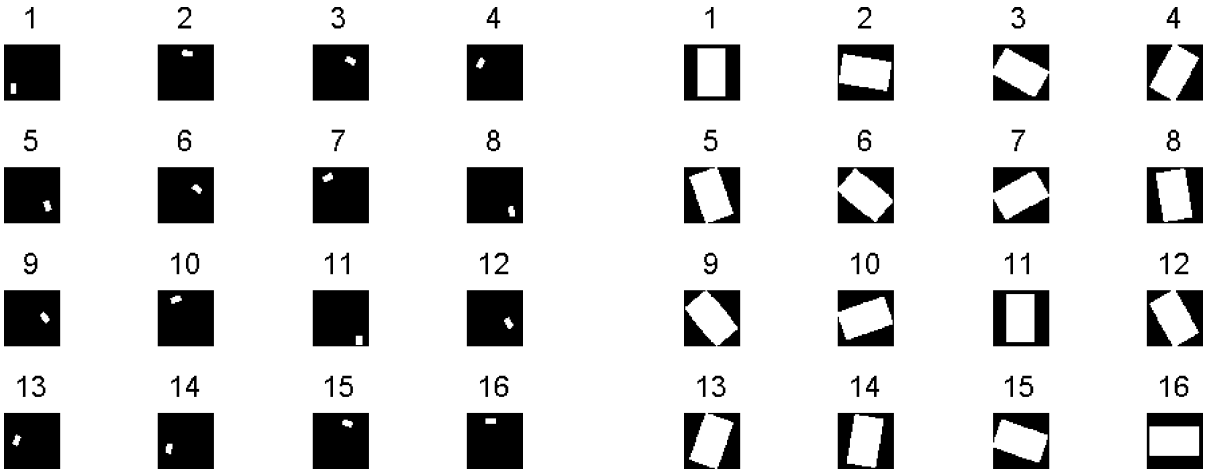

Fig. 18 Unordered video frames

Fig. 19 Mean cancellation and rotation estimation

quite well. We have used it for computing rotations in $\mathbb{R}^3$ for the previous example of a curve in $SE(3)$.

The Euclidean distances between the mean locations of the rectangles found out from the relative positions of the rectangle is the first part of the distance metric. Next we estimate the rotation angle of the object with respect to a fixed inertial frame. For this purpose first we register the objects with their means, see Fig. 19. An observation reveals that if we overlap the registered rectangles the area of the overlapping region provides a good estimate of the rotation angle. In fact for $\theta > \arctan(\frac{b}{a})$, the overlapped area is $\frac{a^2}{\sin\theta}$, where a is the shorter side of the rectangle. This clearly indicates that as θ increase the overlapping area decreases upto $\theta = \pi/2$. For calculating the area we count the number of lattice points (pixels) inside the overlapping regions. Finally with the estimate for θ combined with the Euclidean distance between means give the $d(F_1, F_2)$. Using sequential search with known initial frame we are able to re-order the frames as shown in Fig. 20. Even if we do not know the

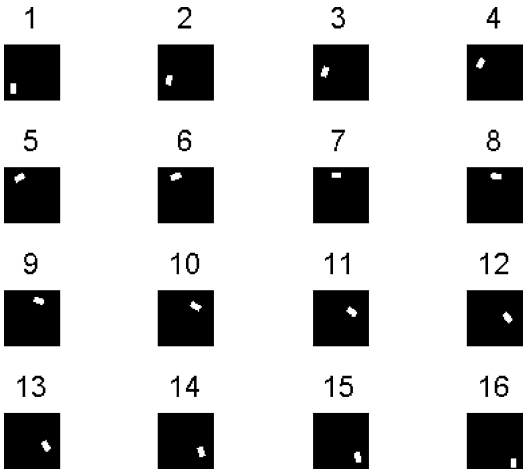

Fig. 20 Ordered video frames

initial frame, MST computes the correct connections of the frames and gives a correct ordering upto end points.

Let us reconsider the distance metric on $SE(2)$ given by (6). If we scale the three axis properly the problem of curve reconstruction in $SE(2)$ reduces to the problem of curve reconstruction in $\mathbb{R}^3$ and we may use all the non-uniform sampling schemes and Voronoi diagram based reconstruction algorithms. As an example we have used NN-CRUST to reconstruct the curve above in the motion sequence and we get the correct ordering as expected.

7 Conclusion

We proved that the MST gives the correct geodesic polygonal approximation to the smooth, closed and simple curves in Riemannian manifolds if the sample is dense enough and we work inside the injectivity radius. We have worked out a conservative bound on the uniform sampling of the curve. The effect of local topological behavior of the underlying manifold was clearly identified and resolved by working inside the injectivity radius. In general the scheme works for the smooth arcs with endpoints also. We have presented simulations for successfully reconstructed curves in $SE(2)$ and $SE(3)$. We have also shown the applications of the combinatorial curve reconstruction for ordering motion frames in graphics and robotics.

If we work inside the injectivity radius of the underlying manifold we have taken care of topological changes but to take care of geometric changes we need to work inside the convexity radius as prescribed in [15]. We believe that the results of non uniform sampling for curves in $\mathbb{R}^n$ are transferable to the curves in Riemannian manifold with careful modifications. As an extension to this work we would like to work out necessary proofs and carry out simulations to support our belief. The effect of noise on the sampling density and the reconstruction algorithm, in case of curved spaces, will be a challenging question. In future, we wish to work on the problem of curve reconstruction from noisy sample on curved spaces.

Acknowledgements The authors would like to acknowledge Prof. Gautam Dutta for discussions on the proof of the results in this article. The authors would also like to thank the resource center DAIICT for providing references needed for the work carried out. We acknowledge INRIA, Gamma researcher's team, http://www-roc.inria.fr/gamma/gamma/disclaimer.php, for their 3D-mesh files which we have used for simulations. We also like to thank anonymous referees for their constructive comments and suggestions.

Appendix: Exponential and Logarithmic Maps

A1 *Given* $[\omega] \in so(3)$,

$$\exp[\omega] = I + \frac{\sin\|\omega\|}{\|\omega\|}\cdot[\omega] + \frac{1-\cos\|\omega\|}{\|\omega\|^2}\cdot[\omega]^2 \tag{19}$$

A2 *Let* $(\omega, v) \in se(3)$. *Then*

$$\exp\begin{bmatrix}[\omega] & v\\ 0 & 0\end{bmatrix} = \begin{bmatrix}\exp[\omega] & Av\\ 0 & 1\end{bmatrix} \tag{20}$$

where

$$A = I + \frac{1-\cos\|\omega\|}{\|\omega\|^2}\cdot[\omega] + \frac{\|\omega\|-\sin\|\omega\|}{\|\omega\|^3}\cdot[\omega]^2$$

A3 *Given* $\theta \in SO(3)$ *such that* $\operatorname{Tr}(\theta) \neq -1$. *Then*

$$\log(\theta) = \frac{\phi}{2\sin\phi}\left(\theta - \theta^T\right) \tag{21}$$

where ϕ *satisfies* $1 + 2\cos\phi = \operatorname{Tr}(\theta)$, $|\phi| < \pi$. *Furthermore,* $\|\log\theta\|^2 = \phi^2$.

A4 *Suppose* $\theta \in SO(3)$ *such that* $\operatorname{Tr}(\theta) \neq -1$, *and let* $b \in \mathbb{R}^3$. *Then*

$$\log\begin{bmatrix}\theta & b\\ 0 & 1\end{bmatrix} = \begin{bmatrix}[\omega] & A^{-1}b\\ 0 & 0\end{bmatrix} \tag{22}$$

where $[\omega] = \log\theta$, *and*

$$A^{-1} = I - \frac{1}{2}\cdot[\omega] + \frac{2\sin\|\omega\| - \|\omega\|(1+\cos\|\omega\|)}{2\|\omega\|^2\sin\|\omega\|}\cdot[\omega]^2$$

A5 *Let* $\theta_1, \theta_2 \in SO(3)$. *Then the distance* $L = d(\theta_1, \theta_2)$ *induced by the standard bi-invariant metric on* $SO(3)$ *is*

$$d(\theta_1, \theta_2) = \left\|\log\left(\theta_1^{-1}\theta_2\right)\right\| \tag{23}$$

where $\|\cdot\|$ *denotes the standard Euclidean norm.*

A6 *Let* $X_1 = (\theta_1, b_1)$ *and* $X_2 = (\theta_2, b_2)$ *be two points in* $SE(3)$. *Then the distance* $L = d(X_1, X_2)$ *induced by the scale dependent left-invariant metric on* $SE(3)$ *is*

$$d(X_1, X_2) = \sqrt{c\left\|\log\left(\theta_1^{-1}\theta_2\right)\right\|^2 + d\|b_2 - b_1\|^2} \tag{24}$$

where $\|\cdot\|$ *denotes the Euclidean norm.*

References

1. Altafini, C.: The de Casteljau algorithm on se(3). In: Isidori, A., Lamnabhi-Lagarrigue, F., Respondek, W. (eds.) Nonlinear Control in the Year 2000. Lecture Notes in Control and Information Sciences, vol. 258, pp. 23–34. Springer, Berlin (2000). http://dx.doi.org/10.1007/BFb0110205.10.1007/BFb0110205
2. Althaus, E., Mehlhorn, K.: Polynomial time tsp-based curve reconstruction. In: Proc 11th ACM-SIAM Sympos Discrete Algorithms, pp. 686–695 (2000)
3. Althaus, E., Mehlhorn, K., Näher, S., Schirra, S.: Experiments on curve reconstruction. In: Proc. 2nd Workshop Algorithm Eng. Exper, pp. 103–114 (2000)
4. Amenta, N., Bern, M., Eppstein, D.: The crust and the β-skeleton: combinatorial curve reconstruction. Graph. Models Image Process. **60**, 125–135 (1998)
5. Basser, P.J., Pajevic, S., Pierpaoli, C., Duda, J., Aldroubi, A.: In vivo fibre tractography using DT-MRI data. Magn. Reson. Med. **44**, 625–632 (2000)
6. Bougleux, S., Peyre, G., Cohen, L.: Anisotropic geodesics for perceptual grouping and domain meshing. In: ECCV2008, vol. 5303, pp. 129–142 (2008). http://www.springerlink.com/index/t10k26241022w670.pdf
7. do Carmo, M.P.: Riemannian Geometry. Birkhäuser, Basel (1992)
8. Dey, T.K.: Curve and Surface Reconstruction: Algorithms with Mathematical Analysis. Cambridge University Press, Cambridge (2007)
9. Dey, T.K., Kumar, P.: A simple provable curve reconstruction algorithm. In: Proc. 10th Ann. ACM-SIAM Symp. Discrete Algorithms (1999)
10. Edelsbrunner, H.: Shape reconstruction with Delaunay complex. In: LNCS 1380, LATIN'98: Theoretical Informatics, pp. 119–132 (1998)
11. de Figueiredo, L.H., de Miranda Gomes, J.: Computational morphology of curves. Vis. Comput. **11**, 105–112 (1994)
12. Gray, A., Abbena, E., Salamon, S.: Modern differential geometry of curves and surfaces with mathematica. In: Studies in Advanced Mathematics. Chapman & Hall, London (2006)
13. Kim, M.J., Kim, M.S., Shin, S.Y.: A c^2-continuous b-spline quaternion curve interpolating a given sequence of solid orientations. Computer Animation 72 (1995). http://doi.ieeecomputersociety.org/10.1109/CA.1995.393545
14. Kimmel, R., Sethian, J.A.: Computing geodesic paths on manifolds. In: Proc. of National Academy of Sciences, USA, vol. 95, pp. 8431–8435 (1998)
15. Leibon, G., Letscher, D.: Delaunay triangulations and Voronoi diagrams for Riemannian manifolds. In: Symposium on Computational Geometry, pp. 341–349 (2000)
16. Li, J., Hao, P.-w.: Smooth interpolation on homogeneous matrix groups for computer animation. J. Zhejiang Univ. Sci. **7**, 1168–1177 (2006). http://dx.doi.org/10.1631/jzus.2006.A1168.10.1631/jzus.2006.A1168
17. Lucas, B.D., Kanade, T.: An iterative image registration technique with an application to stereo vision. In: Intl. Joint. Conf. on Artificial Intelligence (1981)
18. Mansouri, A.R., Mukherjee, D.P., Acton, S.T.: Constraining active contour evolution via Lie groups of transformation. IEEE Trans. Image Process. **13**(6), 853–863 (2004). http://viva.ee.virginia.edu/publications/04_Constraining.pdf
19. O'Rourke, J.: Computational Geometry in C, 2nd edn. Cambridge University Press, Cambridge (1998)
20. Park, F.C.: Distance metrics on the rigid-body motions with applications to mechanism design. J. Mech. Des. **117**(1), 48–54 (1995)
21. Park, F.C., Ravani, B.: Smooth invariant interpolation of rotations. ACM Trans. Graph. **16**(3), 277–295 (1997)
22. Shoemake, K.: Animating rotation with quaternion curves. SIGGRAPH Comput. Graph. **19**(3), 245–254 (1985). http://doi.acm.org/10.1145/325165.325242
23. Spivak, M.: A Comprehensive Introduction to Differential Geometry, vol. 1. Publish or Perish, Berkeley (1999). http://www.jstor.org/stable/2319112?origin=crossref
24. Wang, Y., Wang, D., Bruckstein, A.M.: On variational curve smoothing and reconstruction. J. Math. Imaging Vis. **37**(3), 183–203 (2010)
25. Zefran, M., Kumar, V., Croke, C.: On the generation of smooth three-dimensional rigid body motions. IEEE Trans. Robot. Autom. **14**(4), 576–589 (1995)

Pratik Shah is currently a faculty member with the LNM Institute of Information Technology (LNMIIT), Jaipur, India. He has earned his Master's degree ('05) from DAIICT and has submitted his Ph.D. thesis to DAIICT. His research interests include signal processing, differential geometry and scientific computing. He has also worked as a senior research fellow ('06–'08) with Naval Science and Technological Laboratory, Vizag, India.

Samaresh Chatterji is a professor with the Dhirubhai Ambani Institute of Information and Communication Technology (DAIICT), Gandhinagar, India. He obtained his Ph.D. in Mathematics from Wayne State University in 1979. His research interests include algebra, discrete mathematics and computer simulations and applications.